

Supporting Information

The role of ECL2 in CGRP receptor activation: a combined modelling and experimental approach

Michael. J. Woolley¹, Harriet A. Watkins², Bruck Taddese³, Z. Gamze Karakullukcu³, James Barwell⁴, Kevin J Smith³, Debbie L. Hay,² David R. Poyner^{4*}, Christopher A. Reynolds^{3*}, Alex. C. Conner^{1*},

¹ Warwick Medical School, University of Warwick, Coventry, CV4 7AL, ² School of Biological Sciences, University of Auckland, 3 Symonds Street, Private Bag 92 019, New Zealand, ³School of Biological Sciences, University of Essex, Wivenhoe Park, Colchester, CO4 3SQ, United Kingdom, and ⁴School of Life and Health Sciences, Aston University, Aston Triangle, Birmingham, B4 7ET.

*To whom correspondence should be addressed.

Index of supplementary tables, supplementary figures and other information

Table 1	pEC ₅₀ values for the CGRP and and AM-mediated increases in cAMP	2
Table 2	Fitted basal and maximum (Emax) stimulation of cAMP	3
Table 3	Cell surface expression of mutants	4
Table 4	The affinity of CGRP for mutant receptors	5
Figure 1	Activation and the conformation of H155 ^{2.43} and F362 ^{7.53} in the active model	6
Figure 2	Concentration-response curves of mutants showing changes in pEC ₅₀	7
Figure 3	Interactions between ECL2 residues and CGRP residues over 100 conformations	8
Figure 4	The conformation of ECL2 in the CLR/CGRP and CLR/AM complex	9
Figure 5	The range of interactions between W283 and other parts of CLR	10
Figure 6	Interactions between AM and ECL2	10
Figure 7	The interaction between CGRP and key residues at the top of TM2	11
Figure 8	The conformation of ECL2 and the orientation of Trp283	12
Figure 9	RMSD, RMSF and secondary structure for the active CLR	13
Figure 10	Active CLR simulations and the ECL2 / W283 conformation	14
Figure 11	The Highest scoring Glide-docked pose of CGRP ₁₋₇	15
Figure 12	The CLR/CTR ECL1 alignment	15
Figure 13	A comparison between the preferred CLR/CGRP model, the best CLR/AM model and the recent class B glucagon and CRF X-ray structures	16
	Molecular dynamics methodology	17
	Docking methodology	17
	MD simulations and the orientation of W283	17
	Sequence analysis supports the CGRP1-7 docked pose orientation	18
	Help for downloading the structures from ftp.essex.ac.uk/pub/oyster/	19
	References	19

Supplementary Tables

Supplementary Table 1. pEC₅₀ values for the CGRP and AM-mediated increases in cAMP on ECL2 mutants of the CGRP receptor.

Mutant	CGRP		AM	
	(WT) pEC ₅₀	Mutant pEC ₅₀	(WT) pEC ₅₀	Mutant pEC ₅₀
A271L	10.5 ± 0.27 (4)	10.4 ± 0.41 (4)	7.57 ± 0.12 (5)	7.56 ± 0.13 (5)
I272A	10.2 ± 0.59 (3)	10.2 ± 0.58 (3)	7.88 ± 0.08 (5)	7.97 ± 0.13 (5)*
A273L	10.5 ± 0.33 (3)	9.99* ± 0.25 (3)	8.22 ± 0.16 (4)	8.07 ± 0.15 (4)*
R274A	9.51 ± 0.35 (3)	7.74* ± 0.17 (3)	8.19 ± 0.18 (3)	#nc
S275A	8.81 ± 0.19 (3)	8.66 ± 0.11 (3)	8.32 ± 0.24 (3)	7.99 ± 0.14 (3)
L276A	8.81 ± 0.19 (3)	8.70 ± 0.19 (3)	8.32 ± 0.24 (3)	8.10 ± 0.28 (3)
Y277A	9.41 ± 0.13 (3)	8.44 ± 0.26* (3)	7.53 ± 0.15 (4)	7.31 ± 0.08 (4)
Y278A	9.83 ± 0.16 (5)	8.75 ± 0.08** (5)	7.76 ± 0.05 (3)	7.54 ± 0.11 (3)
N279A	9.85 ± 0.19 (4)	9.65 ± 0.27 (4)	7.84 ± 0.08 (6)	7.66 ± 0.08 (6)
D280A	9.90 ± 0.04 (3)	8.01 ± 0.13* (3)	8.27 ± 0.15 (7)	#nc
N281A	9.65 ± 0.22 (3)	9.83 ± 0.34* (3)	8.32 ± 0.12 (5)	8.48 ± 0.11 (5)
C282A	9.41 ± 0.73 (3)	8.32 ± 0.64* (3)	8.07 ± 0.07 (3)	7.35 ± 0.17** (3)
W283A	9.37 ± 0.76 (4)	<6	8.22 ± 0.11 (8)	#nc
I284A	8.81 ± 0.18 (3)	7.70 ± 0.10* (3)	7.91 ± 0.23 (4)	6.89 ± 0.12* (4)
S285A	10.1 ± 0.19 (5)	9.41 ± 0.27* (5)	8.26 ± 0.10 (4)	7.89 ± 0.04* (4)
S286A	8.91 ± 0.24 (3)	8.98 ± 0.17 (3)	8.02 ± 0.29 (3)	8.38 ± 0.30 (3)
D287A	8.91 ± 0.24 (3)	8.03 ± 0.05* (3)	8.32 ± 0.24 (3)	7.77 ± 0.38 (3)
T288A	9.85 ± 0.35 (4)	8.46 ± 0.28** (4)	8.18 ± 0.16 (3)	7.32 ± 0.09* (3)
H289A	9.85 ± 0.26 (3)	9.82 ± 0.10 (3)	8.30 ± 0.16 (4)	8.68 ± 0.17 (4)
L290A	10.6 ± 0.19 (3)	9.72 ± 0.17* (3)	8.27 ± 0.21 (3)	8.07 ± 0.13 (3)
L291A	10.6 ± 0.19 (3)	9.93 ± 0.23* (3)	8.41 ± 0.16 (5)	8.40 ± 0.20 (5)
Y292A	10.4 ± 0.29 (3)	10.0 ± 0.37 (3)	8.22 ± 0.16 (4)	8.03 ± 0.11 (4)
I293A	10.6 ± 0.19 (3)	10.3 ± 0.22 (3)	7.45 ± 0.18 (3)	7.65 ± 0.15 (3)
I294A	10.4 ± 0.23 (4)	10.7 ± 0.39 (4)	8.25 ± 0.23 (5)	8.08 ± 0.11 (5)

Numbers in parentheses refer to the number of individual experiments and values presented are mean ± s.e.m. *p < 0.05, **p < 0.01, by paired Student's t-test or repeated measures ANOVA followed by Dunnett's test as appropriate #nc No Curve; reduction in cAMP was too great to fit a curve. Grey shading represents significant changes in pEC₅₀ value.

Supplementary Table 2. Fitted basal and maximum (Emax) stimulation of cAMP produced in response to CGRP and AM on the ECL2 mutants of the CGRP receptor.

	CGRP		AM	
	Basal	Emax	Basal	Emax
A271L	6.24 ± 3.91 (4)	107.3 ± 5.24 (4)	2.21 ± 1.82 (5)	97.4 ± 12.23 (5)
I272A	-1.10 ± 5.02 (3)	105.3 ± 3.39 (3)	4.02 ± 2.15 (5)	99.9 ± 0.01 (5)
A273L	4.63 ± 2.13 (3)	104.1 ± 5.66 (3)	4.80 ± 1.65 (4)*	143.5 ± 27.9 (4)
R274A	-3.26 ± 4.19 (3)	67.1 ± 29.05 (3)	nc	nc
S275A	3.87 ± 4.86 (3)	91.3 ± 8.96 (3)	12.5 ± 4.87 (3)	123.0 ± 16.4 (3)
L276A	8.06 ± 3.25 (3)	106.5 ± 7.29 (3)	7.79 ± 3.71 (3)	81.3 ± 3.3 (3)*
Y277A	-8.46 ± 2.47 (3)	90.8 ± 7.21 (3)	4.07 ± 1.12 (4)**	79.9 ± 11.1 (4)**
Y278A	-0.91 ± 7.54 (5)	93.48 ± 12.0 (5)	3.95 ± 1.80 (3)	68.3 ± 4.94 (3)**
N279A	-1.23 ± 6.14 (4)	93.5 ± 3.20 (4)	7.41 ± 3.84 (6)	104.8 ± 18.8 (6)
D280A	9.73 ± 2.58 (3)	103.4 ± 5.97 (3)	nc	nc
N281A	9.91 ± 0.85* (3)	112.3 ± 5.25 (3)	17.9 ± 9.38 (5)	185.5 ± 40.4 (5)
C282A	-8.97 ± 35.9 (3)	85.2 ± 10.1 (3)	4.28 ± 2.34 (3)	70.7 ± 6.34 (3)**
W283A	nc	nc	nc	nc
I284A	14.9 ± 8.28 (3)	114.7 ± 9.63 (3)	14.7 ± 5.24 (4)*	42.0 ± 10.6 (4)***
S285A	15.2 ± 4.55 (5)	93.4 ± 6.56 (5)	4.99 ± 2.63 (4)	99.9 ± 16.23 (4)
S286A	8.42 ± 8.74 (3)	104.2 ± 9.62 (3)	6.08 ± 2.20 (3)	119.1 ± 9.0 (3)
D287A	15.7 ± 11.1 (3)	118.5 ± 7.64 (3)	6.04 ± 4.05 (3)	101.8 ± 15.7 (3)
T288A	17.4 ± 5.17 (4)	116.1 ± 3.86 (4)	5.94 ± 3.35 (3)	92.9 ± 8.33 (3)
H289A	8.44 ± 13.0 (3)	106.9 ± 15.9 (3)	6.24 ± 11.9 (4)	122.4 ± 31.0 (4)
L290A	5.34 ± 7.83 (3)	105.1 ± 1.75 (3)	2.14 ± 1.23 (3)	97.7 ± 15.0 (3)
L291A	12.5 ± 5.44 (3)	105.9 ± 1.76 (3)	3.61 ± 1.83 (3)	147.4 ± 37.5 (3)
Y292A	15.4 ± 10.3 (3)	110.90 ± 0.94* (3)	4.52 ± 3.12 (4)	134.2 ± 20.6 (4)
I293A	10.5 ± 9.00 (3)	109.1 ± 3.85 (3)	-7.28 ± 9.25 (3)	122.1 ± 21.1 (3)
I294A	21.8 ± 2.93* (4)	109.8 ± 1.51* (4)	7.28 ± 9.25 (3)	99.4 ± 15.2 (3)

Numbers in parentheses refer to the number of individual experiments and values are percentages of the fitted basal and Emax seen on WT receptors and are presented as mean ± s.e.m. *p < 0.05, **p < 0.01, by paired Student's t-test or repeated measures ANOVA followed by Dunnett's test as appropriate, #nc No Curve; Reduction in cAMP was too severe to fit a curve. Grey shading represents significant changes in values. Basal values represent cAMP production in the absence of CGRP.

Supplementary Table 3. Cell surface expression of mutants, measuring HA-CLR in the presence of RAMP1.

Mutant	n	Expression (%)	Mutant	n	Expression (%)
A271L	3	99.1±7.4	W283A	3	69.8±1.0
I272A	3	134.8±12.2	I284A	4	62.8±8.1
A273L	3	104.2±3.9	S285A	8	54.6±6.5
R274A	4	93.2±6.1	S286A	4	74.1±12.8
S275A	4	78.9±14.1	D287A	4	95.8±10.8
L276A	3	89.9±9.0	T288A	3	94.2±2.3
Y277A	4	82.8±9.8	H289A	3	74.8±0.1
Y278A	6	97.7±20.6	L290A	3	83.2±7.4
N279A	4	82.9±13.9	L291A	3	103.7±4.1
D280A	4	83.5±18.6	Y292A	3	93.9±4.5
N281A	4	103.3±24.8	I293A	3	103.7±7.7
C282A	3	67.8±2.1	I294A	3	100.8±9.1

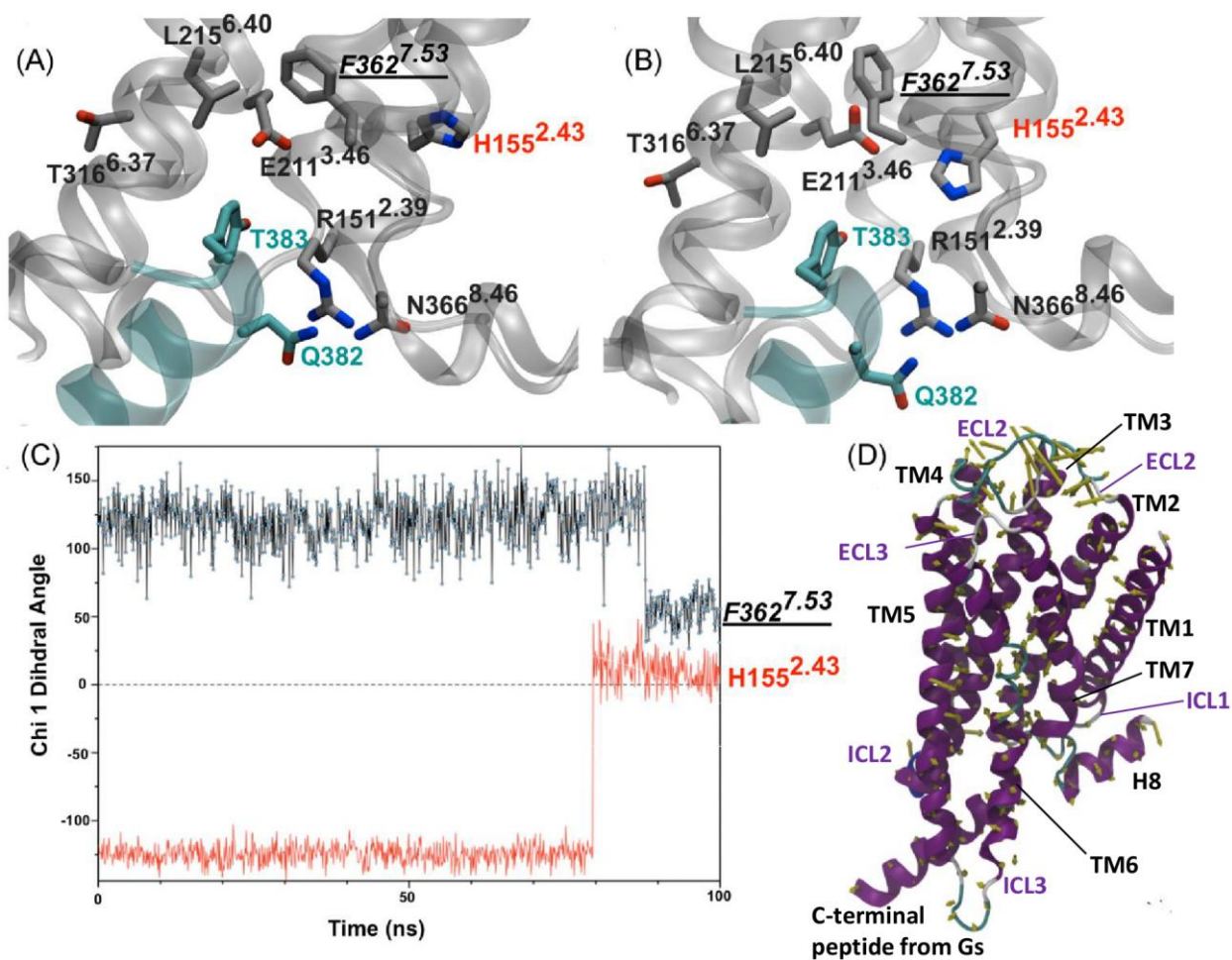
Values are expressed as a percentage of WT receptor, as determined by ELISA and are presented as mean ± s.e.m.

Supplementary Table 4. The affinity of CGRP for mutant receptors.

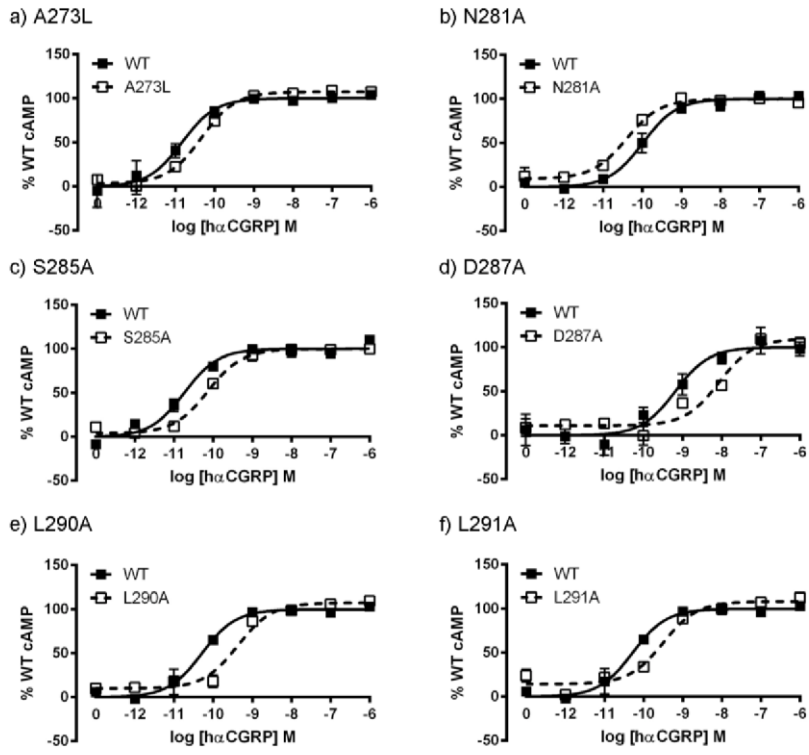
Mutant	pKd
WT	9.18 ± 0.05
R274A	7.77 ± 0.25 **
Y277A	8.99 ± 0.53
Y278A	7.75 ± 0.39 **
D280A	8.39 ± 0.64 *
C282A	8.47 ± 0.07 *
W283A	8.13 ± 0.25 **
S285A	Undetectable
T288A	8.32 ± 0.43 *

Values are mean ± SEM from three determinations. Kd and Bmax values determined from ¹²⁵[I]-CGRP radioligand binding. *, ** significantly different from WT, P <0.05 and P <0.01, as assessed by paired Student's t-test.

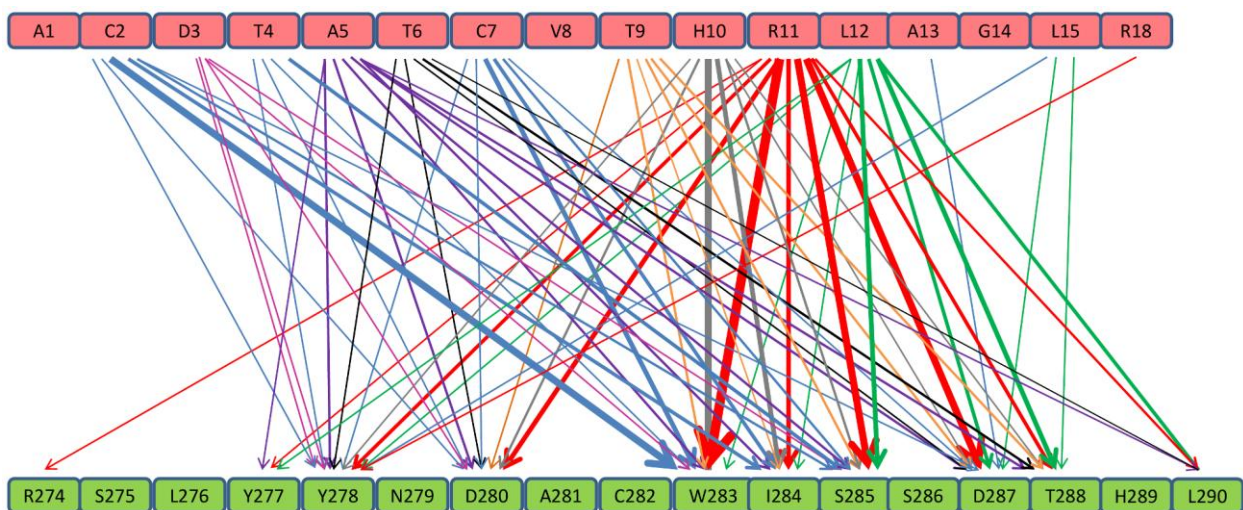
Supplementary Figures



Supplementary Figure 1. The conformation of H155^{2.43} and F362^{7.53} in the active model, (A) before and (B) after the conformational change that introduces inactive character into the active model. (C) The variation in the χ_1 dihedral angle for H^{2.43} and F^{7.53}; the conformational change in F^{7.53} at 80 ns may be associated with the onset of inactive character. (D) Principle components for the active model determined over the course of the simulation. The direction and magnitude of the arrows indicate the motion indicated by the 1st principle component; this magnitude is largest for ECL2.

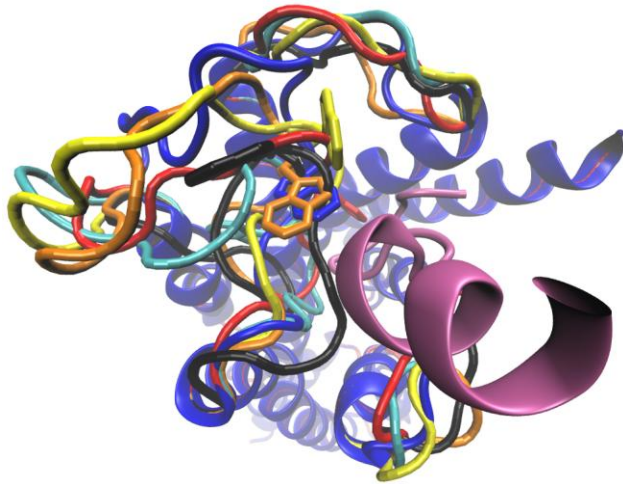


Supplementary Figure 2. Concentration-response curves of mutants showing changes in pEC_{50} in response to CGRP. Representative curves are shown from experiments repeated at least 3 times. The curves are normalised to the fitted E_{max} for CGRP on the WT receptor, which is defined as 100%.

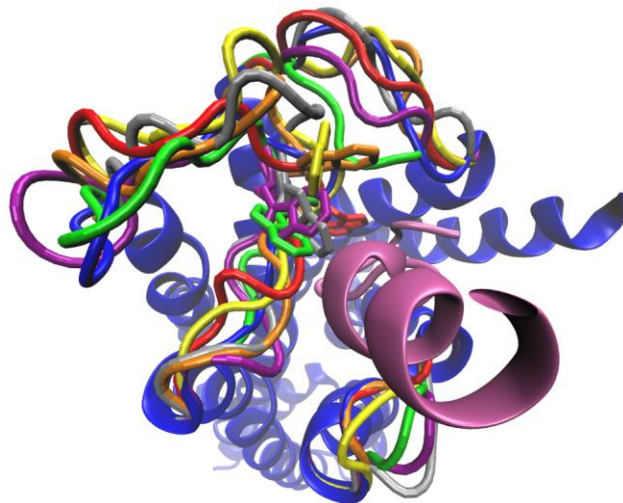


Supplementary Figure 3. The interactions between ECL2 residues and CGRP residues as observed over the full set of 100 ECL2 conformations; the thickness of the line is broadly in line with the frequency of the interactions. (For clarity interactions observed in fewer than 10 structures were omitted from Figure 4C). The coloured lines indicate interactions of specific CGRP residues: D³ (magenta), A⁵ (purple), T⁶ (black), T⁹ (orange), H¹⁰ (grey), R¹¹, R¹⁸ (red), L¹², L¹⁵ (green).

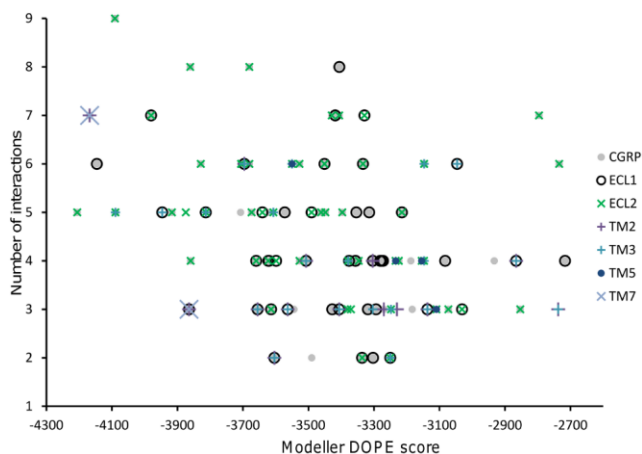
(A)



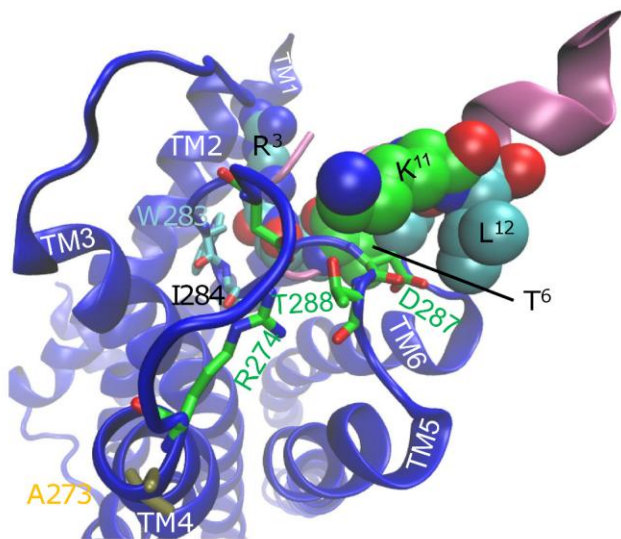
(B)



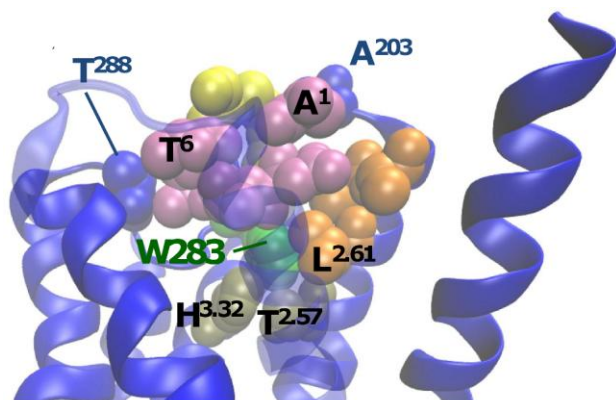
Supplementary Figure 4. The conformation of ECL2 in the CLR/CGRP and CLR/AM complex. (A) CGRP (mauve) interacting with ECL2 of CLR, with interactions involving Y²⁷⁸, D²⁸⁰, W²⁸³, I²⁸⁴, D²⁸⁷ and T²⁸⁸. W²⁸³ interacts with V^{2.58} and L^{2.61} on TM2 and H^{3.32} on TM3. A¹ of CGRP interacts with A²⁰³ in CLR and T⁶ of CGRP interacts with T²⁸⁸. (B) AM (mauve) interacting with ECL2 of CLR, with interactions involving R²⁷⁴, Y²⁷⁸, D²⁸⁰, W²⁸³, I²⁸⁴, D²⁸⁷ and T²⁸⁸. W²⁸³ interacts with V^{2.58} and L^{2.61} on TM2 and H^{3.32} on TM3. The glycine at the equivalent of position 1 of CGRP interacts with A²⁰³ in CLR and threonine at the equivalent position 6 of CGRP interacts with D²⁸⁷. The full set of structures is available from ftp.essex.ac.uk/pub/oyster/CLR_ECL2_2013/CLR_ECL2_structures.tar.gz



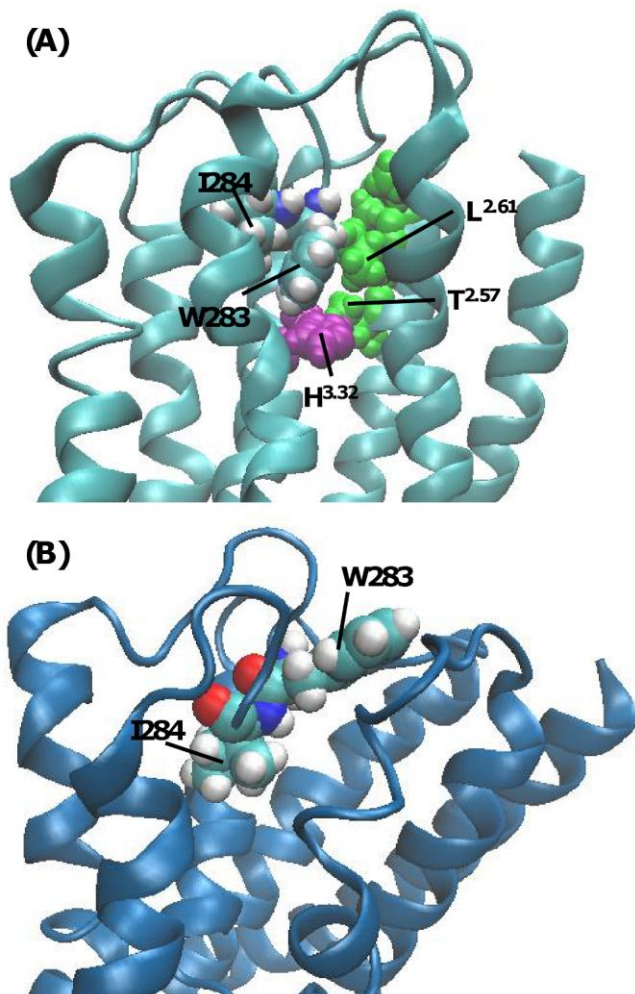
Supplementary Figure 5. The range of interactions between W283 and other parts of CLR over the 100 Modeller conformations. Many of the conformations where W283 interacts with ECL1 can be ignored on the basis of mutagenesis results (Barwell et al., 2011). Conformations that do not involve interactions between T⁶ and D280, D287 or T288 can also be ignored – see Figure 4B.



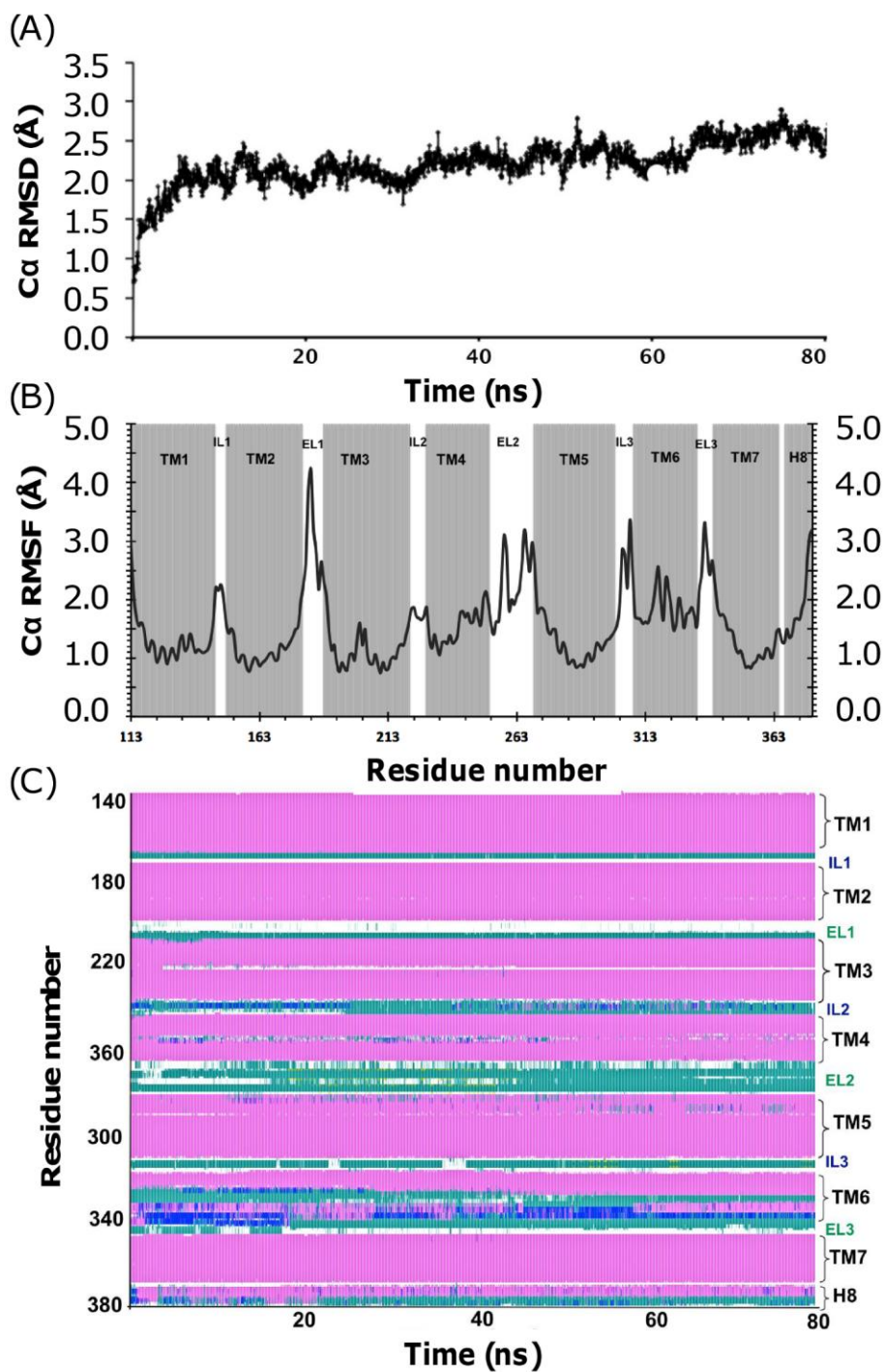
Supplementary Figure 6. Interactions between AM and ECL2. The ECL2 polar residue interactions (green C-atoms) include Y278 with K¹¹, D280 with K¹¹, D287 with T⁶, V⁹, K¹¹ and L¹² and T288 with K¹¹; the ECL2 hydrophobic residue interactions (cyan C atoms) include W283 with the hydrophobic part of R³ as well as residues on TM2 and TM3 and I284 with F⁴.



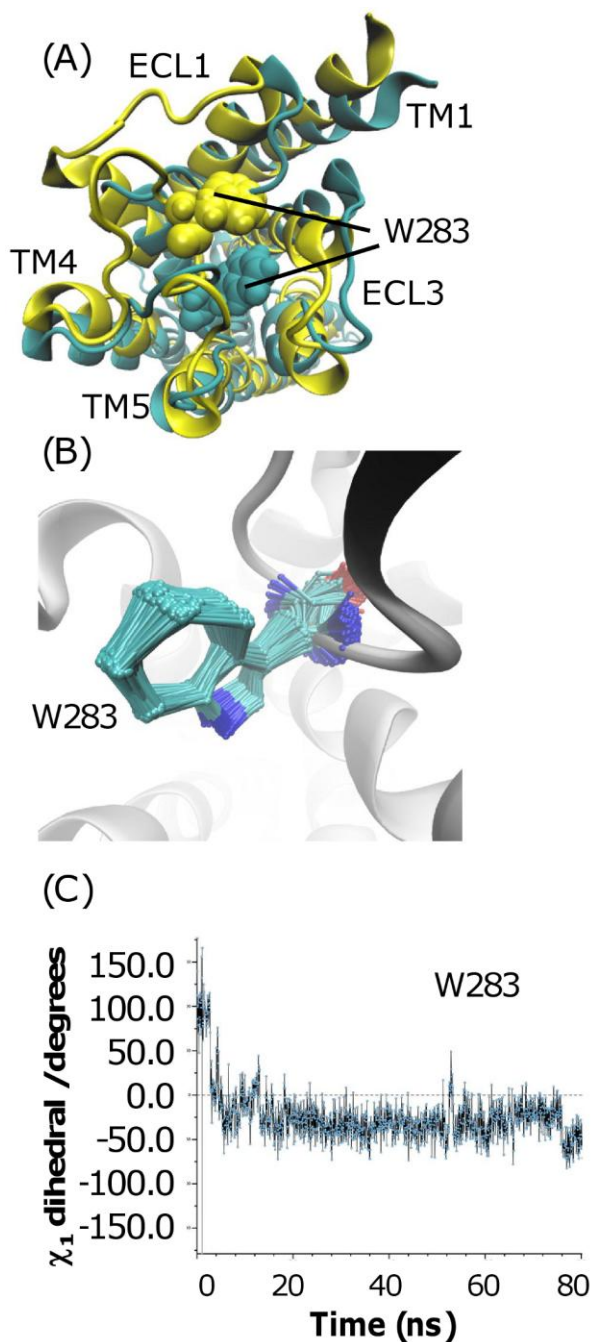
Supplementary Figure 7. The interaction between CGRP₁₋₇ (mauve) and key residues at the top of TM2 (L^{2.61}, V^{2.64} and A^{2.65}; orange) is shown. W283 (ECL2, green) is shown interacting with T^{2.57} (yellow) and H^{3.32} (tan). Resides A¹ and T⁶ reside close to Ala203 and Thr288 respectively (blue). The CGRP disulfide bond is shown in yellow. The loop conformation shown here for ECL2 was a high scoring (i.e. favoured) conformation. TM7 is shown as transparent.



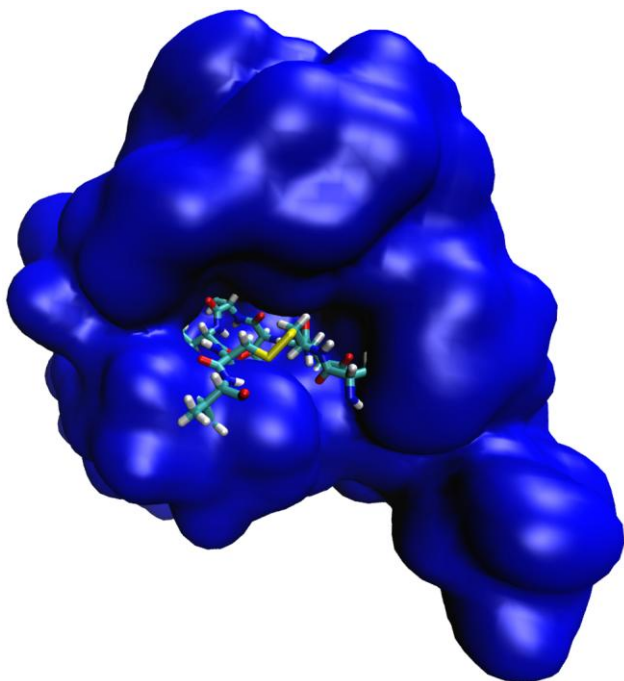
Supplementary Figure 8. The conformation of ECL2 and the orientation of Trp283. (A) A typical inactive conformation with Trp283 and Ile284 shown in spacefill, coloured according to atom type. Hydrophobic residues on TM2 that when mutated show reduced cAMP production in response to CGRP are shown in green spacefill; Trp283 is able to interact with TM2 in this vertical conformation. His^{3.32} has similar mutation effects and is shown in purple. (B) A typical active conformation of Trp283 and Ile284 shown in spacefill, coloured according to atom type; here Trp283 adopts lateral conformation and interacts with hydrophobic residues in ECL1 rather than with TM2. These ECL2 loop conformations were produced by modeller.



Supplementary Figure 9. RMSD, RMSF and secondary structure for the active CLR simulation (larger simulation box). (A) The RMSD for the TM helical backbone. (B) the RMSF of the Ca atoms. The two peaks for ECL2 correspond to the regions either side of the CW motif. (C) The variation in secondary structure throughout the simulation. The elements of secondary structure are denoted as follows: helix, pink; turn, green; 3₁₀-helix, blue; sheet, yellow and coil, white.



Supplementary Figure 10. Active CLR simulations and the ECL2 / W283 conformation. (A) A comparison of the end point of the first active simulation (Desmond software/OPLS force field, cyan) with the end point of the second simulation (NAMD software/CHARMM force field, yellow). During the simulation, W283 moves from an internal position where it interacts with the top of TM2 to a more external position where it loses this TM2 interaction. (B). Local superposition of the ECL2 backbone showing the various conformations of W283. (C) The variation of the W283 χ_1 dihedral angle during the simulation.

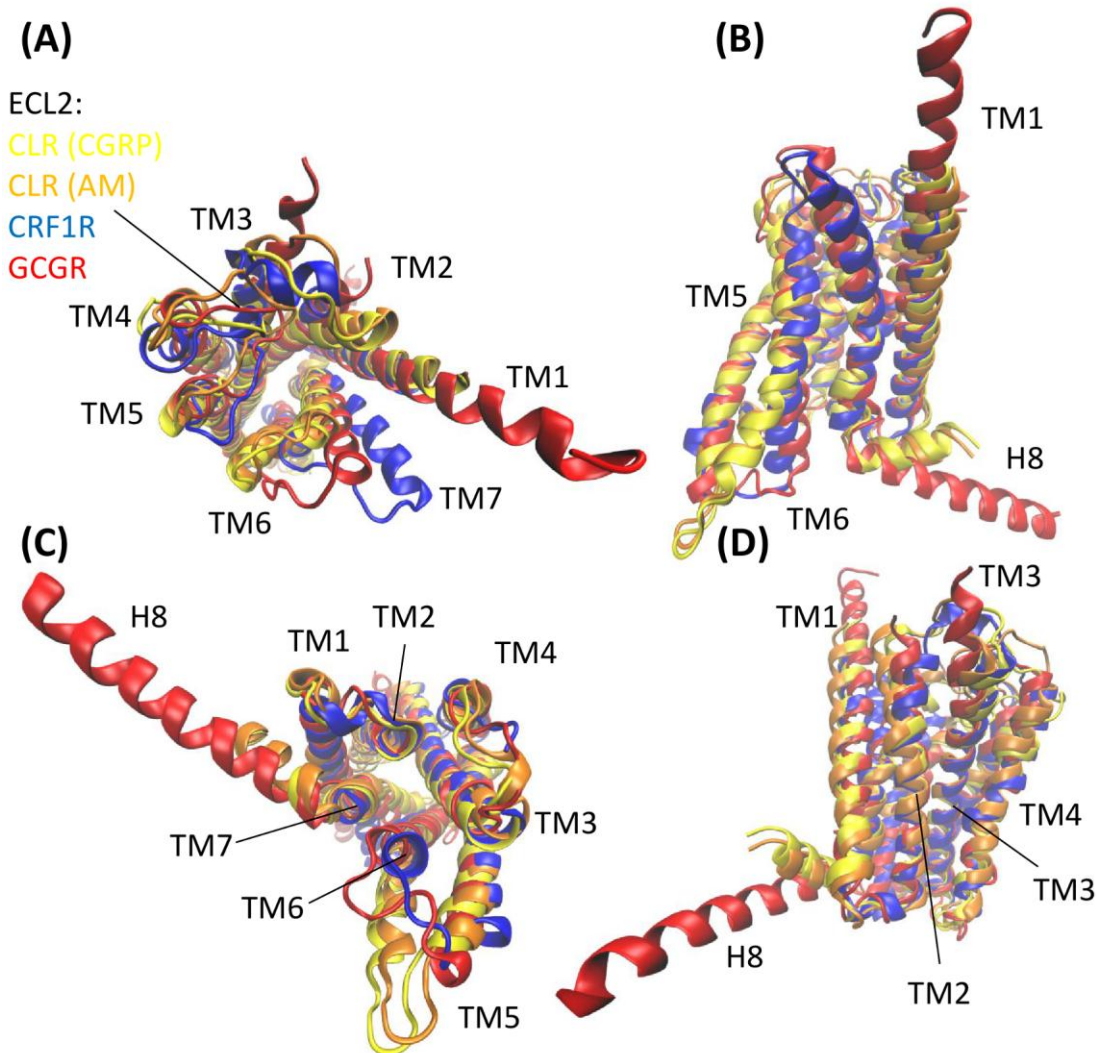


Supplementary Figure 11. The Highest scoring Glide-docked pose of CH₃CO-CGRP₁₋₈-NHCH₃ (licorice model, CPK colours) interacting with the active CLR model (blue surface).

<i>CALR_HUMAN</i>	L	G	C	Q	R	V	T	L	H	K	N	M	F	L	T	Y	I	L	N	S	M	I	I	I	I	H	L	V	E	V	V	P	N	G	E	L	V	R	R	D
<i>CALR_RABIT</i>	L	G	C	Q	R	V	T	L	H	K	N	M	F	L	T	Y	I	L	N	S	M	I	I	I	I	H	L	V	E	V	V	P	N	G	E	L	V	R	R	D
<i>CALR_CAVPO</i>	L	G	C	Q	R	V	T	L	H	K	N	M	F	L	T	Y	I	L	N	S	M	I	I	I	I	H	L	V	E	V	V	P	N	G	E	L	V	R	K	D
<i>CALR_MOUSE</i>	L	S	C	Q	R	V	T	L	H	K	H	M	F	L	T	Y	I	L	N	S	I	I	I	I	I	H	L	V	E	V	V	P	N	G	D	L	V	R	R	D
<i>CALR_RAT</i>	L	S	C	Q	R	V	T	L	H	K	N	M	F	L	T	Y	I	L	N	S	I	I	I	I	I	H	L	V	E	V	V	P	N	G	D	L	V	R	R	D
<i>CALR_PIG</i>	I	S	C	Q	R	V	T	L	H	K	N	M	F	L	T	Y	V	L	N	S	I	I	I	I	V	H	L	V	V	I	V	P	N	G	E	L	V	K	R	D
<i>CGRR_HUMAN</i>	L	S	C	Q	R	I	T	L	H	K	N	L	F	F	S	F	V	C	N	S	V	V	T	I	I	H	L	T	A	V	A	N	N	Q	A	L	V	A	T	N
<i>CGRR_RAT</i>	L	S	C	Q	R	I	T	L	H	K	N	L	F	F	S	F	V	C	N	S	I	V	T	I	I	H	L	T	A	V	A	N	N	Q	A	L	V	A	T	N

-----|-----

Supplementary Figure 12. The CLR/CTR ECL1 alignment, reproduced using Jalview [1]. Position 203 (CLR numbering) is D/E in CTR and A in CLR and is marked by a vertical bar. The residues are colour coded according to their properties as follows: blue, positive; red, negative or small polar; purple, polar; cyan, polar aromatic; green, large hydrophobic; yellow, small hydrophobic. This corresponds to the ‘Taylor’ scheme, as implemented in Jalview.



Supplementary Figure 13. A comparison between the preferred CLR/CGRP model (yellow), the best CLR/AM1 model (in terms of agreement with glucagon receptor, GCGR, ECL2 conformation) (orange), the GCGR X-ray structure (red) and the corticotropin releasing factor 1 (CRF1R) X-ray structure (blue). (A) The conformation of ECL2 for CLR (yellow/orange) is similar to that of GCGR (red), especially for CLR/AM (orange). Interestingly there are significant differences between ECL2 of GCGR and CRF1R, suggesting the precise ECL2 conformation is receptor specific. ECL1 is missing from GCGR; the CLR and CRF1R conformations differ, partly because ECL1 in CLR interacts with the peptide. (B) There are differences at the intracellular end of TM6 as CLR (yellow/orange) is an active model whereas GCGR and CRF1R are inactive. There some differences in H8 (missing from CRF1R). (C) The intracellular region is similar except for the outward movement of TM6 in the CLR active models. (D) The main differences in TM1 - TM4 are at the top of the helices and can be related to the peptide interaction. In some places CLR is closer to GCGR or CRF1R than they are to each other, except in TM1, which takes a multitude of conformations in class A structures. The greater similarity between GCGR and CLR in TM3 and TM4 may arise because of the CRF lysozyme fusion. The RMSD was evaluated over residues 140-163 (TM1), 172-195 (TM2), 224-250 (TM3), 226-285 (TM4) and 390-400 (TM7) (GCRG residue numbers, and their equivalent in other structures). TM5 and TM6 were omitted because of their role in activation; residues at the extracellular end of TM7 were omitted because of the variable outward tilt in CLR, GCGR and CRF1R. The RMSD was 1.9 Å between GCGR and CLR and 1.7 Å, an between GCGR and CRF1R; the CLR structures were deposited on the University of Essex ftp server on 28.6.2013; the CRF1R and GCGR structures were released on 17.7.2013 and 24.7.2013 respectively [2,3].

Molecular dynamics methodology

The initial models [4] were equilibrated for 5 ns through molecular dynamics simulations of CLR embedded in a lipid bilayer of 68 POPC lipids and 6498 SPC water molecules using Desmond [5] and the OPLS 2005 force field [6] and simulated for a further 100 ns. ECL2 is critical to CGRP and AM binding but modeling loop conformations is difficult because of sampling issues [7]. We have extended these simulations of the inactive [4] and active CLR to 192 POPC lipids and 9238 and 10554 water molecules respectively using Namd [8] and the CHARMM_22 force field [9] with the CMAP correction [10]. The simulations with the docked CGRP peptide were predictably unstable in the absence of the N-terminus of CLR and the RAMP (i.e. the docked CGRP drifted away) and so these simulations were run in the absence of CGRP but in the presence of the Gs C-terminal peptide to help maintain the active conformation. The second set of simulations with a larger simulation box were equilibrated for 20 ns and run for 80 ns. Further details are given in [4]

Docking methodology

End groups were added to CGRP₁₋₇ to create CH₃CO-CGRP₁₋₈-NH-CH₃, which was used in the docking. A 10 Å³ inner docking box was constructed between TM2, TM3, TM5/TM6 and TM7, with H^{3.32} near the centre; a 30 Å³ outer docking box, with Y^{3.40} near the bottom, was also defined. The peptide was allowed complete flexibility; limited flexibility within the otherwise rigid receptor was modelled by scaling the van der Waals radii of non-polar atoms by 0.8. Residues S175 – L191 of ECL2 were moved clear of the binding site using the interactive molecular graphics structure sculpting feature in Maestro [39] since the original MD-derived loop conformation prevented docking. The only constraint on the docking, which is inherent to Glide and was set through the choice of the box sizes, was that the centre of the ligand cannot move out of the inner box (except in the subsequent minimization). Five thousand poses (within 100 kcal mol⁻¹ of the minimum energy) were initially generated and the best 400 were kept for minimization using the OPLS all atom force field and of these, the 8 poses with the lowest (best) glide score were reported (10 were requested: to differ by an RMSD of > 0.5% and a max atom displacement of > 1.3 Å). These 8 poses differed essentially only in the orientation of the end-capping groups (CH₃-CO, NH-CH₃) and the T⁶ side chain; the end groups were removed prior to extending CGRP beyond residue 7. The best scoring pose (by both the glide score and Emodel, which includes the conformational energy) was verified by sequence analysis, as described below.

Molecular dynamics simulations and the orientation of W283

Molecular dynamics simulations of CLR in a POPC bilayer showed that the conformation of ECL2 is broadly similar in both the inactive and active receptor states, in that the hydrophobic

residues W283 and I284 dip into the helical bundle. However, the orientation of the W283 side-chain differed in these two cases, giving rise to both vertical (illustrated in Figure 6) and lateral conformations, (Illustrated in Supplementary Figure 8). To some extent the conformation given by the active simulations is artificial as it was generated in the absence of CGRP, giving the tryptophan residue space to sample areas that would normally not be available or would be difficult to sample. The loop generation, which was carried out using the active structure in the presence of CGRP, generated conformations of ECL2 that gave rise to both the lateral and the vertical orientations of W283. W283 interacted with ECL1 in a number of these modeller generated conformations (and in the simulations – see Supplementary Figure 10A), but while there is a significant mutagenesis effect for W283 (Figure 1, Supporting Table 1), residues in ECL1 generally have much smaller effects on CGRP activity, indicating that W283 does not interact with ECL1 [11]. The orientation of W283 in the simulation of the inactive state, coupled with the mutagenesis data, gave support to the preference for the vertical conformation.

The RMSF overall all residues and the helical backbone RMSD over the 80 ns simulation time for the NAMD active simulation is given in Supplementary Figure 9. The RMSD, at $\sim 2.0 - 2.5 \text{ \AA}$ shows relatively minor overall changes considering the change in force field. The main fluctuations, as expected are in the loop regions, including ECL2 (Supplementary Figure 9B), and the secondary structure remains relatively constant, as shown in Supplementary Figure 9C. The main feature in Supplementary Fig 9C is the disruption of helical character in TM6 associated with the bend required for activation. No conformational changes were observed for H^{2.43} or F^{7.53} during these NAMD simulations. Supplementary Figure 10A shows that during the NAMD simulation, W283 moves from a more internal position where it faces the top of TM2 to a more external position where this interaction is lost. Supplementary Figure 10B/C shows that the χ_1 angle of the W283 changes very little during this time, and so although the position of W283 can vary for relatively similar ECL2 conformations, the position of W283 is driven more by the local movement of ECL2 than by changes in χ_1 ; visual inspection shows that this movement of ECL2 in the simulations is far less than that generated by Modeller. However, the absence of the CGRP peptide makes further analysis of the orientation of W283 difficult and so a full MD analysis of the behaviour of ECL2 and W283 is beyond the scope of this work. Rather, this will need to wait until more is known about the way the N-terminus, RAMP and CGRP peptide interact with the CLR helical bundle.

Sequence analysis supports the CGRP₁₋₇ docked pose orientation

Because ECL2 is important in peptide binding and in activation, prior to analysing the ECL conformations, it is important to ensure that the peptides are docked in accordance with the known experimental information. In this section, evidence supporting our proposed orientation of CGRP (and AM) is discussed.

Selectivity filter

The highest scoring docked pose for CH₃CO-CGRP₁₋₈-NH-CH₃ is shown in Supplementary Figure 11. In the presence of RAMP1, both CLR and CTR, bind CGRP with high affinity [2, 3], whereas the CGRP receptor has very low affinity for amylin; consequently, there must be a selectivity “filter” present in CLR but not CTR that discriminates against amylin in the presence of RAMP1.

For all known amylin sequences, the first residue is always lysine (i.e. K¹). The N-terminus of CGRP is group-conserved as a small hydrophobic/weakly polar residue (alanine or serine) across all known sequences [4]. If this switch at residue 1 of amylin/CGRP contributes to the selectivity filter, then it is likely to be reflected by a correlated change in the sequence of the ECLs of CLR and CTR. There are very few positions that would allow this. The best candidate is in ECL1 (Supplementary Figure 12) where A203 in CLR (D/E in CTR) is a potential partner for A¹ of human alpha CGRP; this is supported by our earlier mutagenesis data, which showed that mutating this residue to leucine increased the affinity of CGRP [1]. A197^{2.63} in CLR could have a similar role, but in CTR its equivalent would not be a good partner for K¹ of amylin as it is a valine residue in porcine CTR.

Adrenomedullin N-terminal extensions

The AM peptide has an N-terminal extension that is apparently not essential for binding and receptor activation and does not appear to interfere with these processes [5]. On the assumption that AM and CGRP bind in a similar fashion, the correctly docked peptides should be able to accommodate an N-terminal extension and thus should not be in a sterically crowded environment.

Help for downloading the structures

The structures can be obtained from:
ftp.essex.ac.uk/pub/oyster/CLR_ECL2_2013/CLR_ECL2_structures.tar.gz. On linux/unix systems, the tar file can be uncompressed using *gunzip* and the structures extracted using *tar -xvf CLR_ECL2_structures.tar.gz*; the pdb files can then be uncompressed using *gunzip* (*gunzip file.pdb.gz*). On windows systems, it is probably sufficient to use successive double clicks on the archive to see the tar file and its contents which can be extracted (using jZip) by highlighting the pdb files (not file.pdb.gz) and using the *Extract files* command, which is under *Actions*. Users without jZip can download 7ZIP (www.7-zip.org/) for free.

References

1. Clamp, M., Cuff, J., Searle, S.M., & Barton, G.J. 2004 The Jalview Java alignment editor. *Bioinformatics* **20**, 426-427.
2. Hollenstein, K., Kean, J., Bortolato, A., Cheng, R.K., Dore, A.S., Jazayeri, A., Cooke, R.M., Weir, M., & Marshall, F.H. 2013 Structure of class B GPCR corticotropin-releasing factor receptor 1. *Nature* **499**, 438-443.

3. Wang, C., Wu, H., Katritch, V., Han, G.W., Huang, X.P., Liu, W., Siu, F.Y., Roth, B.L., Cherezov, V., & Stevens, R.C. 2013 Structure of the human smoothed receptor bound to an antitumour agent. *Nature* **497**, 338-343.
4. Vohra, S., Taddese, B., Conner, A.C., Poyner, D.R., Hay, D.L., Barwell, J., Reeves, P.J., Upton, G.J., & Reynolds, C.A. 2013 Similarity between class A and class B G-protein-coupled receptors exemplified through calcitonin gene-related peptide receptor modelling and mutagenesis studies. *J R. Soc Interface* **10**, 20120846.
5. Bowers, K. J., Chow, E., Xu, H., Dror, R. O., Eastwood, M. P., Gregersen, B. A., Klepeis, J. L., Kolossvary, I., Moraes, M. A., Sacerdoti, F. D. *et al.* (2006) Tampa, Florida).
6. Kaminski, G.A., Friesner, R.A., Tirado-Rives, J., & Jorgensen, W.L. 2001 Evaluation and reparametrization of the OPLS-AA force field for proteins via comparison with accurate quantum chemical calculations on peptides. *J. Phys. Chem. B* **105**, 6474-6487.
7. Goldfeld, D.A., Zhu, K., Beuming, T., & Friesner, R.A. 2011 Successful prediction of the intra- and extracellular loops of four G-protein-coupled receptors. *Proc Natl. Acad. Sci. U. S. A* **108**, 8275-8280.
8. Phillips, J.C., Braun, R., Wang, W., Gumbart, J., Tajkhorshid, E., Villa, E., Chipot, C., Skeel, R.D., Kale, L., & Schulten, K. 2005 Scalable molecular dynamics with NAMD. *J Comput Chem* **26**, 1781-1802.
9. Brooks, B.R., Bruccoleri, R.E., Olafson, B.D., States, D.J., Swaminathan, S., & Karplus, M. 1983 Charmm - A Program for Macromolecular Energy, Minimization, and Dynamics Calculations. *J. Comput. Chem.* **4**, 187-217.
10. Buck, M., Bouguet-Bonnet, S., Pastor, R.W., & Mackerell, A.D., Jr. 2006 Importance of the CMAP correction to the CHARMM22 protein force field: dynamics of hen lysozyme. *Biophys. J* **90**, L36-L38.
11. Barwell, J., Conner, A., & Poyner, D.R. 2011 Extracellular loops 1 and 3 and their associated transmembrane regions of the calcitonin receptor-like receptor are needed for CGRP receptor function. *Biochim. Biophys. Acta* **1813**, 1906-1916.